RSC Advances

PAPER

View Article Online
View Journal | View Issue

Cite this: *RSC Adv.*, 2025, **15**, 9320

Exploring the dermal safety of green-synthesized Ag–TiO_2 nanocomposites for topical applications†

Archana Rana, *[ab] Shweta Parashar,[c] Diksha Singh,[c] Kavita Singh,[c] Debabrata Chanda,[bc] Anirban Pal,[bc] Ritu Srivastava [ab] and Shailesh Narain Sharma*[d]

We investigated Ag–TiO_2 nanocomposites (NCs) synthesized using leaf extracts of *Azadirachta indica* and *Mangifera indica* for topical applications. The Ag–TiO_2 NCs were first characterized by their spherical shapes, with sizes ranging from 20–26 nm to 5–6 nm, and a zeta potential value between −27 and −23 mV. DLS analysis revealed average particle sizes of 671 nm and 573 nm for Ag–TiO_2 NCs synthesized from *A. indica* and *M. indica*, respectively. The MICs of the nanocomposites were determined *via* dilution in both Gram-positive and Gram-negative bacteria to determine the optimal concentration for dermal applications. The cytotoxicity assay (MTT) of ATN and ATM compounds at MICs of 312.5 μg mL^{-1}, 625 μg mL^{-1}, and 1250 μg mL^{-1} showed that they were nontoxic to fibroblast cells. Further assessments of acute and subacute dermal safety were conducted on Charles Foster rats with NCs applied at 625 μg mL^{-1}, 3125 μg mL^{-1}, and 6250 μg mL^{-1} concentrations. Observations were made for any signs of dermal toxicity using behavioural and physical indices. In acute dermal toxicity, the NCs were applied once, and in subacute dermal toxicity, NCs were applied once daily for 28 days and observed for any sign of dermal toxicity using observation indices like behavioural changes, edema scores, and erythema scores. Post-experiment analyses of body weight, serum biochemistry, oxidative stress, and hematological profiles revealed that the nanocomposites exhibited significant antimicrobial activity. Notably, the safety evaluations indicated no adverse changes, suggesting these NCs are well-tolerated for dermal applications and show great promise for future topical applications.

Received 19th November 2024
Accepted 7th March 2025

DOI: 10.1039/d4ra08199d

rsc.li/rsc-advances

1. Introduction

Nanomaterials are an emerging technology with various applications in science, particularly in the field of topical formulations. Cosmetic and skin-related products have become an essential part of many people's daily routines owing to growing awareness of the harmful biological effects caused by ultraviolet (UV) radiation, skin allergies and infections. Exposure to the sun can lead to serious issues, such as skin cancer, photoaging, DNA damage, erythema, and increased reactive oxygen species in the skin.[1] In today's world, sunscreens are expertly crafted with UV filters—both organic and inorganic—to provide essential protection against harmful UV radiations. Organic UV filters, such as octocrylene, oxybenzone, and avobenzone, have been on the market for decades. However, they can trigger severe skin allergies due to the accumulation of unwanted substances in the adipose tissue. Conversely, inorganic filters stand out for their remarkable benefits, including broad spectrum protection, exceptional photostability, and a unique whitening effect. These qualities not only enhance their effectiveness but also affirm their safety for all skin types. Available in an array of different forms—oils, lotions, gels, and convenient roll-on applications—these products not only safeguard the skin but also ensure a luxurious, enjoyable experience in the sun.[2] TiO_2 NPs have previously been recognized as an inert material used in the cosmetics industry, and they are considered safe for use on the skin, as authorized by the EU's Scientific Committee on Consumer Safety (SCCS), with a maximum concentration of 25%. This safety is likely owing to the high surface area of TiO_2 NPs, which enhances transparency in visible light while reflecting and scattering UV rays.[3] Thus, while NPs have gained popularity in sunscreen formulations, mounting concerns about their potential toxicity have emerged, sparking ongoing discussions about their safety on human skin.[4] Recent studies have highlighted the remarkable potential of titanium dioxide (TiO_2) and AgNPs, which are traditionally synthesized through a variety of physical and chemical methods involving reducing agents.[5] However, there is a growing interest towards more sustainable and cost-effective approaches—

[a]*CSIR-National Physical Laboratory, Dr K. S. Krishnan Marg, New Delhi 110012, India. E-mail: microarchana91@gmail.com*
[b]*Academy of Scientific and Innovative Research (AcSIR), Ghaziabad 201002, India*
[c]*CSIR-Central Institute of Medicinal and Aromatic Plants (CSIR-CIMAP), Lucknow, India*
[d]*Delhi Technological University, Shahbad Daulatpur Village, Rohini, 110042, India. E-mail: shaileshnarainsharma@dtu.ac.in*

† Electronic supplementary information (ESI) available. See DOI: https://doi.org/10.1039/d4ra08199d

known as green methods—that not only reduce energy waste but also eliminate the risks associated with toxic substances.

This innovative shift toward green synthesis not only enhances the safety of nanoparticle production, but also unveils the potential for these nanoparticles in medical treatments, owing to the abundance of rich phytochemicals that they harness.[6] This evolution in synthesis techniques promises a more sustainable future for nanotechnology, merging environmental stewardship with cutting-edge medical applications. Green-synthesized NPs have shown remarkable effectiveness in topical applications.

Kwek *et al.* studied the effect of extracted TiO_2 NPs from sunscreens tested *in vitro* and *ex vivo* on human epidermal skin cells, showing lower cytotoxic activity than in the pristine form.[7]

Similar studies have been conducted by Nilavuk Karasi *et al.* to synthesize TiO_2 NPs using *Capparis zeylanica* leaf extract and assess their effect on wound healing in Swiss albino mice. The results demonstrated that a higher dose of TiO_2 NPs concentration exhibited 99% wound healing on the 13th day. The histopathological studies have not shown any side effects, but produced more cells on the epithelium layer.[8] Similar studies have been conducted for heparin–polyvinylalcohol@TiO_2 nanocomposite bandages to treat burn injuries. The incorporation of the TiO_2 NPs porosity, degradation rate, and antimicrobial activity increases the cell viability to enhance the wound healing properties.[9] AgNPs are well known for their strong antimicrobial properties due to their ability to release silver ions, which can bind to and disrupt the cell walls and membranes of bacteria and other microorganisms. AgNPs have been employed as bactericidal agents in hygiene and medical purposes, and increasingly as nanomedicine for treating and cleaning burns and diabetic wounds, as well as for purification of equipment. Studies show AgNPs have antibacterial properties and absorb in the UV range. The current studies revealed that AgNPs protect skin from UVB rays in both mouse models and cell cultures.[10] Green synthesized AgNPs were added to pluronic F-127 hydrogels at different concentrations to study their effect on the wounds of mice. The closure of the wound was confirmed on the 10th day with 95% healing, and the treatment did not observe any skin irritation and can be used as a topical ointment.[11]

Kim *et al.* (2016) studied the dermal and eye toxicity of AgNPs in rats and rabbits and did not observe any sign of erythema, oedema, or irritation effects on the eyes.[12] Recently, some studies have been published by Elatter *et al.* on Ag@TiO_2, and Ag@SeO_2 core/shell NCs synthesized by *Beta vulgaris* L. extract for *R. solani* and *S. sclerotiorum* fungi. The reported values found for Ag@TiO_2 NCs were 314, 624 μg mL^{-1} and 930, 1390 μg mL^{-1}.[13] The studies reveal that Ag@TiO_2 NCs were (one and a half times) more efficacious than Ag@SeO_2 NCs. Citrus lemon leaf extract-mediated AgNPs have been applied as an ointment to treat the wounds of Sprague Dawley rats, and it could be used for the treatment of human wounds.[14] Ag–TiO_2 NCs are composite materials that combine different phases of silver nanoparticles (AgNPs) and titanium dioxide nanoparticles (TiO_2 NPs). These nanocomposites have attracted significant attention due to their unique properties, which are different from those of their components. The AgNPs that occupy the surface of TiO_2 decrease the band gap and increase the photocatalytic properties, and are proposed to be effective nanocomposites in sunscreen.[15] The combination of AgNPs and TiO_2 NPs can lead to synergistic effects, such as enhanced photocatalytic activity, antibacterial properties, and improved electrical conductivity. Ag–TiO_2 NCs have potential applications in various fields, such as water purification, food packaging, and medical devices. They can be used to disinfect surfaces, prevent the growth of bacteria and other microorganisms, and reduce the risk of infections.[16] Ag–TiO_2 NCs@PF-127 HNRs were studied against 4T1 cancer cells, and showed 90% inhibition against the cells at a concentration of 120 mg mL^{-1} under UV radiation.[17]

Despite numerous studies, TiO_2 NPs face several challenges, including high recombination rates of electron–hole pairs, a small band gap energy, and low absorption capacity. To address these issues, researchers have doped TiO_2 NPs with various metal nanoparticles, such as silver (Ag), gold (Au), and iron (Fe). This doping helps to reduce the band gap without compromising the crystallinity of the TiO_2 NPs, and facilitates the diffusion of charge carriers on the surface of the nanoparticles.[18]

The photocatalytic activity of Ag–TiO_2 NPs is enhanced at the interface between Ag and TiO_2 NPs when exposed to UV light. When UV light is present, photoinduced electrons are transferred from the silver nanoparticles (Ag NPs) to the titanium dioxide nanoparticles TiO_2 NPs, increasing their photocatalytic activity. The electrons that accumulate on the surface of the TiO_2 NPs react with oxygen or other molecules to produce superoxide radicals. Additionally, the holes generated during this process can oxidize hydroxyl groups (–OH) or water (H_2O) to create powerful oxidizing radicals, such as hydroxyl radicals ($^{\bullet}OH$). Moreover, TiO_2 NPs can be oxidized by these strong oxidizing radicals ($^{\bullet}OH$), resulting in the production of carbon dioxide CO_2 and several other oxidized intermediates.[19] The integration of AgNPs into TiO_2 NPs significantly diminishes the recombination of e^-/h^+ pairs, ultimately extending the lifespan of Ag–TiO_2 NCs. This remarkable enhancement owes its effectiveness to the captivating surface plasmon effect of AgNPs, which facilitates the transport of electrons from TiO_2 NPs to AgNPs.[20] Inorganic NPs (sunblock) were measured with SPF to reduce the erythema after evaluating the rate of absorption, toxicology, and skin reactions on human skin.[21] Recent studies on Ag/TiO_2 NPs (400 μg mL^{-1}) reveal that, when combined with blue light, there is a 42.79% reduction in cell viability in the A431 skin cancer cell line after 45 minutes, compared to using nanoparticles and light separately.[22] Ag-doped TiO_2 NPs studied on human cancer (liver) cell lines showed better results with the addition of AgNPs, as it only focused on destroying cancer cells.[23] Several studies show that TiO_2 NPs reduce the release of AgNPs, enhancing antimicrobial activity and decreasing health problems and pollution. It is highly used as a hydrogel for wound dressing, cosmetics, antimicrobial agents and semiconductors. These well-known studies promote for skin repairment and wound healing which indicate harmless process to human usage proved *via in vivo* and *in vitro*.[24]

In this study, we synthesized green Ag–TiO_2 NCs using extracts from medicinal plants, specifically *Azadirachta indica* (*A. indica*, also known as neem) and *Mangifera indica* (*M. indica*,

as mango in India), which are commonly found in Asian countries. The synthesized Ag–TiO_2 NCs were assessed for their effects on the cytotoxicity assay (MTT) fibroblast cell line. They were determined to be nontoxic at concentrations up to twice the minimum inhibitory concentration (MIC). Additionally, the sub-acute toxicity of Ag–TiO_2 NCs—derived from *A. indica* (ATN = Ag–TiO_2 neem) and *M. indica* (ATM = Ag–TiO_2 mango) extracts—was safe at levels up to five times the MIC. This research paper presents novel findings on the dermal toxicity of Ag–TiO_2 NCs in CF rats, which have not been previously published.

2. Experimental methods and materials

2.1. Materials

A. indica and *M. indica* leaves were collected from the campus of NPL (National Physical Laboratory), New Delhi, India. The precursors used for synthesis include titanium isopropoxide [$Ti(OC_3H_7)_4$], silver nitrate ($AgNO_3$), iodo-nitrotetrazolium bromide and nutrient broth, which were purchased from Sigma-Aldrich chemicals. The microbial strains (*Staphylococcus aureus* MTCC 96, *Staphylococcus hominis* MTCC 657, *Escherichia coli* MTCC 8739, *Salmonella typhimurium* (MTCC 3232) and *Candida albicans* MTCC 183) were procured from Microbial Type Culture Collection (MTCC), Chandigarh, India.

2.2. Preparation of plant extract

The collected leaves of *A. indica* and *M. indica* were appropriately cleaned under tap water to eliminate dust residue. 30 g of each plant (*A. indica* and *M. indica*) leaves were used to prepare the leaf extract using 100 mL of deionized water, and the mixture was heated at 80 °C for 40 min. The reaction mixture was then filtered using Whatman no. 1 filter paper after cooling to room temperature, and stored at 4 °C.

2.3. Synthesis of Ag–TiO_2 NCs using *A. indica* and *M. indica* leaves extract

The green synthesis of Ag–TiO_2 NCs, followed by precursors (0.2 M) titanium(IV) isopropoxide (TTIP–Ti[$OCH(CH_3)_2]_4$) in 30 mL deionized water, was placed in a round-bottom flask stirred at 70 °C for 20 min. Thereafter, 3 mM silver nitrate ($AgNO_3$) solution with 30 mL of leaves extract of *A. indica* and *M. indica* was added slowly to the round-bottom flask with continuous stirring at 70 °C, following the protocol reported by Bhardwaj *et al.*[25] Slowly, the colour of the reaction mixture changed into a light grey color (could be due to the surface plasmon resonance), which indicates the formation of Ag–TiO_2 NCs. The reaction mixture of the NCs solution was centrifuged at 4000 rpm for 30 min to separate the suspended particles. Furthermore, the NCs particles were washed twice with deionized water to remove the extra product. The collected NCs were then dried overnight at 70 °C in the oven. The resulting Ag–TiO_2 NCs were annealed at 400 °C for 2 h to enhance their crystallinity. A schematic of the synthesis of Ag–TiO_2 NCs is shown in Fig. 1(a). Furthermore, the mechanism of Ag–TiO_2 NCs using plant extract is shown in Fig. 1(b). The TTIP reaction with D.I. water produces unstable $Ti(OH)_4$, which is further converted into TiO_2 through the condensation process. The hydroxyl group of phytochemicals (such as ascorbic acid, quercetin, nimbin, benzoic acid propyl ester) is attached to the surface of TiO_2 after the addition of the plant leaf extract. The addition of AgNPs on the surface of TiO_2 NCs is achieved through hydrogen bonding of the OH group of phytochemicals.

2.4. Structural and morphological characterization

Ag–TiO_2 NCs synthesized using plant leaf extract of *A. indica* and *M. indica* were characterized using Raman, SEM, XRD, FTIR, TEM, and UV-vis analysis. XRD (X-ray diffraction) patterns were recorded using a Bruker D-8 Advance X-ray Diffractometer instrument with Cu Kα with $\lambda = 1.54059$ Å, employing a scanning rate of 0.05° s^{-1} in the 2θ range from 10° to 80°. The

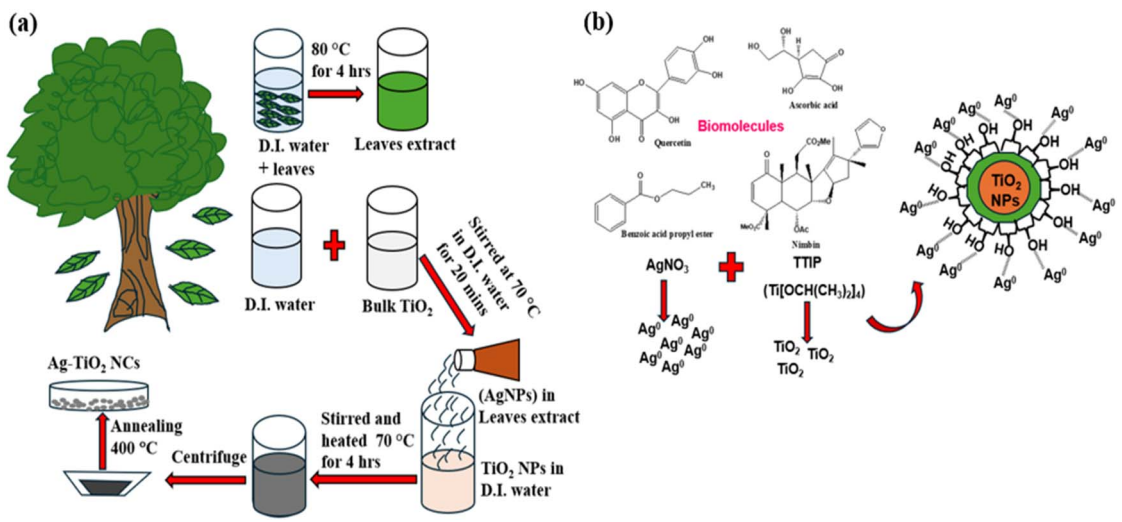

Fig. 1 Schematic of (a) the proposed green synthesis route of Ag–TiO_2 NCs using *A. indica* and *M. indica* leaf extracts and (b) mechanism of Ag–TiO_2 NCs.

absorbance of NCs between 200–800 nm was measured using a UV-vis spectrophotometer (Shimadzu UV-3101). The bandgap energy (E_g) of the NCs obtained may be determined using the following equation:

$$E_g = 1240/\lambda \text{ eV} \quad (1)$$

λ = wavelength (nm) and E_g = band gap (eV).

The powder sample was characterized using Fourier-transform infrared (FTIR) spectra (PerkinElmer FTIR spectrum BX-II analyzer) to investigate the functional groups, which were recorded in the 4000–400 cm^{-1} region.

Raman spectroscopy of NCs was performed using laser excitation at 514.5 nm with an argon ion laser power of approximately 80–100 mW.

The Malvern Panalytical equipment was used to test the stability and hydrodynamic diameter of spherical NCs using dynamic light scattering (DLS). The particle size was estimated using a Malvern (1062761) Zetasizer at 25 °C with a cuvette of 2 mm in an aqueous solution. The biochemical and oxidative stress values were calculated through SpectraMax Plus (384) instrument.

The size and shape of the NPs were assessed using a TEM (Transmission Electron Microscope) instrument from Jeol Ltd [Tokyo, Japan] with an acceleration voltage of 100 kV. The NCs for the TEM investigation were ultrasonicated for 15 minutes before mounting onto a copper grid with carbon coating to dry in the air. The shape of the NCs were studied using a SEM (scanning electron transmission) and EDAX instrument (ZEISS instrument).

2.5. Antimicrobial activities

The Ag and TiO_2 NPs have been studied separately using similar plants and methods for antimicrobial activities on plant pathogens using the disc diffusion method. AgNPs were synthesized using *A. indica* and *M. indica* leaf extract with plant pathogens showing a zone of inhibition of 21 mm (*A. rolfsii* fungi) and 17 mm (*X. oryzae* bacteria) *via* the zone of inhibition disc diffusion method.[26] Similarly, TiO_2 NPs were also synthesized using the same plants and studied against plant pathogens, such as *A. alternata*, *C. gloeosporioides*, *T. harzianum* and *A. rolfsii* fungi and *X. oryzae* as bacteria using the disc diffusion method. Studies on the non-linear optical properties (absorption and refractive index) were also calculated through the Z-scan method.[27] In the current study of Ag–TiO_2 (*A. indica* and *M. indica*), the broth dilution method MIC was performed. Quantitative estimation of microbial growth inhibition by samples was observed by the micro broth dilution assay using 96 well 'U' bottom microtitre plates, as mentioned by Srivastava *et al.*[28] The method employs a two-fold serial dilution technique to assess any given antimicrobial's MIC (Minimum Inhibitory Concentration) under testing. The MIC of the test sample is considered as the concentration at which no colour change is observed, starting from the highest to lowest dilution after incubation of the microtiter plates.

Nutrient broth (100 μL) medium was added to all wells. 100 μL of the sample was added to the first well at a concentration of 5000 mg mL^{-1} diluted with broth medium. The solution was mixed by continuous pipetting (up to 5–6 times) and then transferred 100 μL from the 1st well into the 2nd well. It was serially diluted (2-fold dilution) up to the 10th well for testing as an antimicrobial agent. The schematic of the antimicrobial activity is shown in Fig. 2.

The working inoculum was prepared by diluting 1 mL of the overnight grown culture with 19 mL of sterile broth to achieve a (CFU) of 1×10^6 cfu mL^{-1}. To each well was added 100 μL of this working inoculum, except for the negative control. Column 11 was used for the negative (sterility) control, and column 12 was used for plate sterility with only nutrient broth. After 18 h incubation at 37 °C, plates were evaluated by adding 50 μL of iodo-nitrotetrazolium bromide (stock-1 mg mL^{-1}) dye to achieve a final concentration of 0.02 mg mL^{-1}. The well exhibiting no growth in each row corresponded to that antimicrobial agent's MIC (μg mL^{-1}). The MIC values (μg mL^{-1}) recorded in this study are the mean of three experiments performed in replicates.

3. Cytotoxicity assay (MTT) of ATN and ATM in the fibroblast cell line

3.1. Principle

In 1983, Mosmann introduced the MTT assay, a standard method for assessing cell viability and cytotoxicity. This assay is based on the ability of living cells to reduce yellow tetrazolium salt (MTT) into purple formazan crystals, primarily through the activity of mitochondrial dehydrogenases. Enzymes located in other organelles, such as the endoplasmic reticulum, also play a role in this reduction.[29] Once MTT is taken up by live cells *via* endocytosis, it is metabolized and converted into insoluble formazan crystals, which are transported back to the cell surface, forming needle-like structures. These insoluble crystals are then dissolved using a solubilizing agent, such as DMSO, acidified ethanol, or SDS in diluted hydrochloric acid. The resulting solution is measured using a spectrophotometer at 570 nm to determine the level of cell viability.

3.2. Method

Fibroblast cell lines were cultured in a growth medium (DMEM with 10% heat-inactivated fetal bovine serum), and seeded at a density of 0.5×10^4 cells per well in a 96-well plate. These cells were allowed to adhere overnight at 37 °C in a 5% CO_2 incubator. Following attachment, the cells were treated with ATN and ATM at concentrations of (312.5 μg mL^{-1} (1/2× of MIC), 625 μg mL^{-1} (1× of MIC), and 1250 μg mL^{-1} (2× of MIC)), along with the vehicle control (DMSO), for 12 hours in a culture medium supplemented with 1% serum. After the treatment, 20 μL of MTT solution (prepared from a 5 mg mL^{-1} stock in PBS, 12 mM MTT) was added to each well and incubated for 4 hours. The MTT-containing medium was then carefully removed, and the formed formazan crystals were solubilized in 100 μL of DMSO for 10 minutes, resulting in a blue-coloured solution. Cell viability was assessed by measuring the absorbance of the formazan solution at 570 nm using a spectrophotometer. The

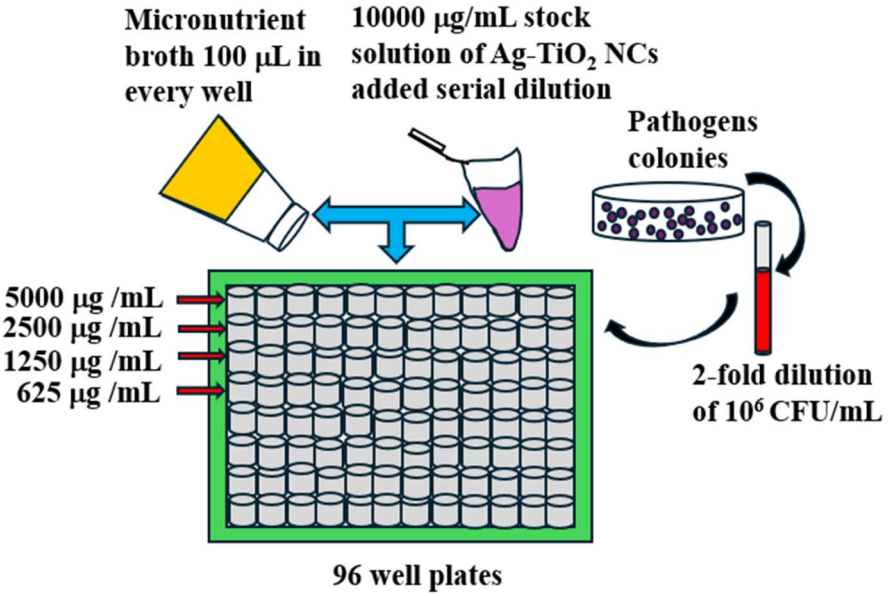

Fig. 2 Antimicrobial activity of Ag–TiO_2 NCs synthesized using *A. indica* and *M. indica* leaf extracts.

intensity of the color was directly proportional to the cell viability, and the viability was expressed as the percentage of survival. Each test was performed with ($n = 4$), and the data were presented as the mean ± SEM ($n = 4$).

4. Mixing of Ag–TiO_2 NCs (*A. indica* and *M. indica*) in sesame oil

Ag–TiO_2 NCs (*A. indica* and *M. indica*) having proven MIC were considered for evaluation of dermal toxicity and were accurately weighed. The MIC (µg mL^{-1}) was considered as × and in dermal toxicity, we have chosen 1×, 5×, and 10× concentrations for our study after suspending the NCs in sesame oil.

4.1. *In vivo* dermal toxicity

Animal studies were carried out according to protocols approved by the Institutional Animal Ethics Committee (IAEC) for Animal Facility, CSIR-CIMAP, Lucknow, UP, India (CIMAP/IAEC/2020-23/22), following the recommendations of the OECD test guidelines for dermal toxicity and FHSA regulations. Before commencing the study, the animals were familiarized with the experimental condition for one complete week (22 °C and a 12 hour dark/light cycle). The animals were given adequate rat feed and drinking water *ad libitum*. In acute dermal toxicity, 8 male and 8 female Charles Foster rats were taken. Following a week of acclimatisation, the animals were divided into 4 groups each with 2 male and 2 female rats (to obtain 8 spots of 1 square inch for the dermal application in each group). The lateral side of the abdominal region was clipped of hair and cleanly shaven with a marked area of a square inch on each side of the rats for applications of the NCs. Group 1 was considered as control, whereas groups 2 through 4 were considered the experimental groups, and were treated with the NCs at 1×, 5×, and 10× of MIC of the NCs. A similar grouping of animals and application procedure of NCs was followed for assessing the sub-acute dermal toxicity, wherein the test substance was applied once daily for 28 days.

4.2. Acute and subacute dermal toxicity

Ag–TiO_2 NCs were used at 1×, 5×, and 10× of MIC to evaluate the toxicity of the NPs. Ag–TiO_2 NCs were solubilized in sesame oil and applied on the marked area of the skin of the CF rats. We observed the animals for 24 hours, while archiving the images of the treated. We determined edema and erythema scores, and calculated the primary irritation index as reported previously.[30]

We performed the sub-acute dermal toxicity tests to determine the adverse effects of Ag–TiO_2 NCs upon repeated dermal exposure to rats. We gave 1×, 5×, and 10× of MIC to the animals for 28 days repeatedly in the marked area of the skin. We took a picture of the marked area before the application of the nanoparticle on day 0. After applying the NCs, the images of the marked area were collected once every 3 days. Animals were regularly monitored for any development of edema and erythema. The irritation index and primary irritation index were calculated for the experimental period of 28 days at 3 day intervals. We shaved the animal twice a week to remove the hairs for the application of the compound until the completion of the experiment. On the 28th day of the experiment, we recorded the body weight of the animals and collected blood from the retro-orbital plexus for biochemistry and hematology. The animals were then sacrificed under high-dose anesthesia (a combination of ketamine at 80 mg kg^{-1} and xylazine at 20 mg kg^{-1} given through the i.p. route), and vital organs like the lung, liver, heart, kidney, spleen, and brain were collected, inspected, and weights were recorded and expressed as absolute and relative organ weight.[31]

4.3. Statistical analysis

Hematological, biochemical, and oxidative stress data were analyzed using statistical calculation in Excel. For these parameters, the data are presented as mean ± standard deviation. The relevant significance level was determined at ($P \leq 0.05$) as applicable. Two-way ANOVA tests were used to examine the differences in the data collected from the groups and evaluate the measurements. We performed all of the experiments in triplicates, and expressed the data as mean ± SEM. Two-way ANOVA was used to calculate the *p*-value.

5. Results and discussion

5.1. Crystallographic structure

XRD was used to determine the crystal structures and phases present in the NCs. In the XRD pattern of Ag–TiO_2 NCs, the peaks observed in the pattern correspond to the diffraction of X-rays by the atoms in the crystal lattice of the NPs. The XRD pattern of silver–TiO_2 NCs shows peaks that correspond to both the silver and TiO_2 phases. In the XRD pattern of the silver–TiO_2 nanocomposites, the peak positions and intensities can provide information about the crystallite size, crystal structure, and composition of the NPs. The XRD pattern of Ag–TiO_2 NC (*A. indica* and *M. indica*) samples is shown in Fig. 3(a). The diffraction peaks at 2θ angles (with corresponding planes) at 25.3° (101), 48.05° (200), 53.9° (105), 55.06° (211), 62.4° (204), 68.76° (220), 70.3° (116), and 75.06° (215), respectively, are attributed to the anatase phase of TiO_2 NPs (JCPDS card no. 21-1272). The XRD pattern of Ag–TiO_2 NCs shows the characteristic peak of Ag at 2θ of 32.3° (111), and 37.9° (004) (JCPDS no. 04-0784).[32] In the sample containing both Ag and TiO_2, the diffraction band of the Ti (004) lattice plane appears at an angle of 37.9°, which is high enough to overlap with the (111) characteristics peak of Ag.[33,34] The XRD pattern in the present study indicates that the dual phases of Ag–TiO_2 NCs have been confirmed by the Ag NPs that were deposited on the surface of the TiO_2 particles. The crystallite size of Ag–TiO_2 NCs (*A. indica* and *M. indica*) was calculated using the Scherrer equation, where β = full width at half maximum, θ = diffraction angle at peak position, and λ = wavelength of X-ray radiation.

$$D = \frac{0.94\lambda}{\beta \cos \theta} \quad (2)$$

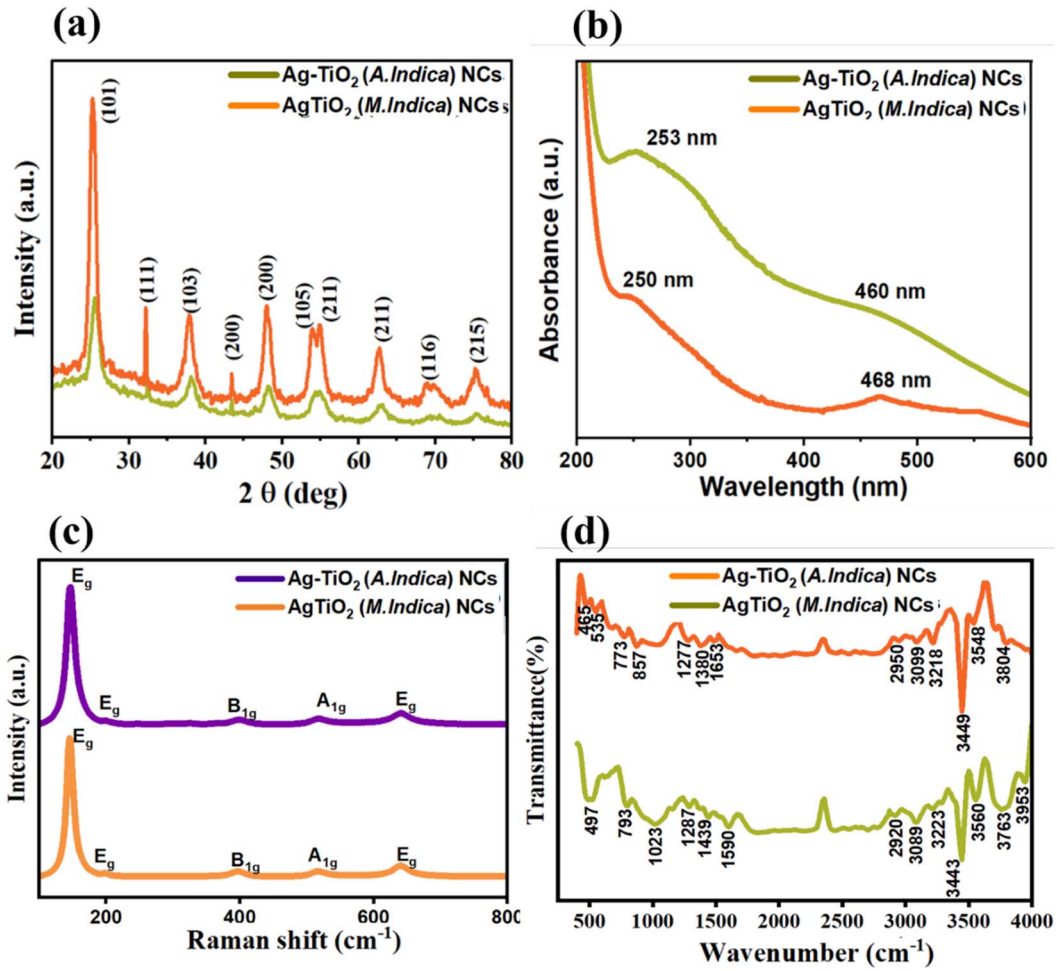

Fig. 3 (a) X-ray diffraction (XRD) patterns of Ag–TiO_2 NCs and (b) UV-vis spectra of Ag–TiO_2 NCs synthesized using *A. indica* and *M. indica* leaf extracts, (c) Raman spectra of Ag–TiO_2 NCs and (d) FTIR spectra Ag–TiO_2 NCs synthesized using leaf extracts of *A. indica* and *M. indica*.

The crystallite size for Ag–TiO_2 NCs was calculated as 7.23 nm and 7.9 nm at 400 °C annealing. Additionally, the XRD pattern exhibits the presence of AgNPs in NCs without coinciding with other peaks of TiO_2 NPs. The high crystalline nature of Ag–TiO_2 NCs is demonstrated by the presence of strong peaks in the data. The XRD pattern shows distinct diffraction peaks of Ag and TiO_2 phases for both samples, with the absence of any other peaks. The characterizations mentioned in the current paper have been studied only for Ag–TiO_2 NCs, whereas the characterization and results for Ag and TiO_2 NPs synthesized using the same plant extracts have been reported earlier for agricultural applications.[26,27]

5.2. Optical properties

The two main UV-vis absorption spectra of Ag–TiO_2 NCs (*A. indica* and *M. indica*) are shown in Fig. 3(b). The absorption bands are related to the electronic transitions in the NPs, which are affected by the size, morphology, and composition of the NPs. The first absorption band in the UV region is associated with the TiO_2 NPs' electronic transitions with a blue shift of 253 and 250 nm (*A. indica* and *M. indica*), which could be due to the AgNPs deposited on the surface of TiO_2 NPs.[35] The second absorption band in the visible region (redshift) is due to the SPR (Surface Plasmon Resonance) of the AgNPs observed at 460 and 468 nm (*A. indica* and *M. indica*).[36] The SPR band of AgNPs observed on the surface of TiO_2 significantly affected the absorption in the visible area of 450–550 nm, and the absorption edge also changes to the visible region for Ag–TiO_2 NCs.[37] The SPR band depends on the size, shape, and concentration of the AgNPs. Ag–TiO_2 NCs (*A. indica* and *M. indica*) was studied in the wavelength range of 200–600 nm. Furthermore, the significant shift in the dielectric property of the surrounding medium marked by the presence of AgNPs was also assigned to these improvements in the optical absorption of the Ag/TiO_2 NCs.[38]

5.3. Raman spectra

Raman spectroscopy is known as an incredibly effectual technique for detecting the vibrational modes of chemical bonds, and can precisely pinpoint the specific crystalline state of materials. In this study, we used this technique to study the Raman spectra of Ag–TiO_2 NCs in the frequency range of 150–800 cm^{-1}, shown in Fig. 3(c). The robust and intense peaks observed at 147 cm^{-1} (E_g (1)) and 199 cm^{-1} (E_g (2)) are optical modes of the anatase phase of TiO_2. The band located at 398 cm^{-1} (B_{1g}), 515 cm^{-1} (A_{1g}), and 641 cm^{-1} (A_{1g}/B_{1g}) assumed a low-frequency shift, corresponding to the LO-phonon in Ag–TiO_2 NCs. For Ag–TiO_2 NCs, all the Raman bands observed were for TiO_2, and the absence of an active band for Ag was due to the crystal symmetry of Ag.[39] However, the oscillations in the Raman spectra could be due to the oxygen atoms further changing the coordination environment of oxygen with the Ti^{4+} atom. Adding Ag atoms to the lattice of TiO_2 to maintain neutrality creates oxygen vacancies and forms Ag–O–Ti NCs.[40] The broadening of the peaks could be possibly attributed to the vibrational amplitudes and particle size.[41]

5.4. Evaluation of functional groups

The FTIR spectrum of Ag–TiO_2 NCs (*A. indica* and *M. indica*) shows the characteristic peaks of fundamental vibrations caused by N–H, O–H, and C–H stretching, measured in the 4000–2500 cm^{-1} range. The stretching vibrations for the absorbed –OH group of water molecules were observed at 3400 cm^{-1}. The C=C and C=O double bonds stretching vibrations are ascribed to the regions 2500–1500 cm^{-1}. The Ti–O–Ti bond stretching vibrations have been identified in the 700–500 cm^{-1} range. The peaks identified at 1287 and 1277 cm^{-1} represent the presence of Ag–O–Ti, which depicts the formation of NCs in Fig. 3(d).[42] The weak peaks observed for TiO_2 NPs were assigned to the lattice vibration range of 1380–1277 cm^{-1}. The Ti stretching vibrations were observed with a prominent peak at 1023 cm^{-1}.

5.5. DLS and zeta potential analysis

Dynamic light scattering is known for detecting the particle size distribution and zeta potential of aqueous nanocomposites of Ag–TiO_2 NCs (*A. indica* and *M. indica*) were determined using dynamic light scattering and a zeta sizer. Typically, the sample is dispersed in a suitable solvent and passed through a laser beam. The scattered light is then detected and analyzed to assess the size of the NPs in the sample. The size of Ag–TiO_2 NCs can vary depending on the synthesis method and the ratio of silver to titanium dioxide. It is important to note that DLS analysis can provide information about the hydrodynamic diameter of the NPs, which can be different from the actual size of the particles measured by TEM. It may be because the NPs are surrounded by a layer of solvent molecules, affecting their size and mobility. The average particle sizes of Ag–TiO_2 NCs (*A. indica* and *M. indica*) were 671 and 573 nm, respectively, as shown in Fig. 4(a) and (b). According to these findings, the presence of AgNPs on the surface of TiO_2 particles may prevent agglomeration.[43]

The zeta potential of these NCs refers to the electric charge that might be present on their surface, which affects their stability and dispersion in a liquid medium. The zeta potential of silver–TiO_2 NCs depends on various factors, such as the size and concentration of the NPs, the pH of the medium, and the presence of other ions. Typically, the zeta potential of these NCs is negative, indicating a repulsive force between them, preventing agglomeration or aggregation of the NPs. A high negative zeta potential is desirable for the stability of the nanocomposites in a liquid medium. The zeta potentials of Ag–TiO_2 NCs (*A. indica* and *M. indica*) were calculated as −27 mV and −23 mV, as shown in Fig. 4(c) and (d).

5.6. Morphological studies (TEM analysis)

The morphology and structure of Ag–TiO_2 NCs were analyzed using TEM, HRTEM and SAED, as shown in Fig. 5(a) and (b), to obtain more details of Ag–TiO_2 NCs (*A. indica* and *M. indica*). The TEM images demonstrate the mesoporous structure and explain the agglomeration of NCs. The TEM analysis of the TiO_2 NPs exhibited averaged particle sizes of 20–26 nm, which were made

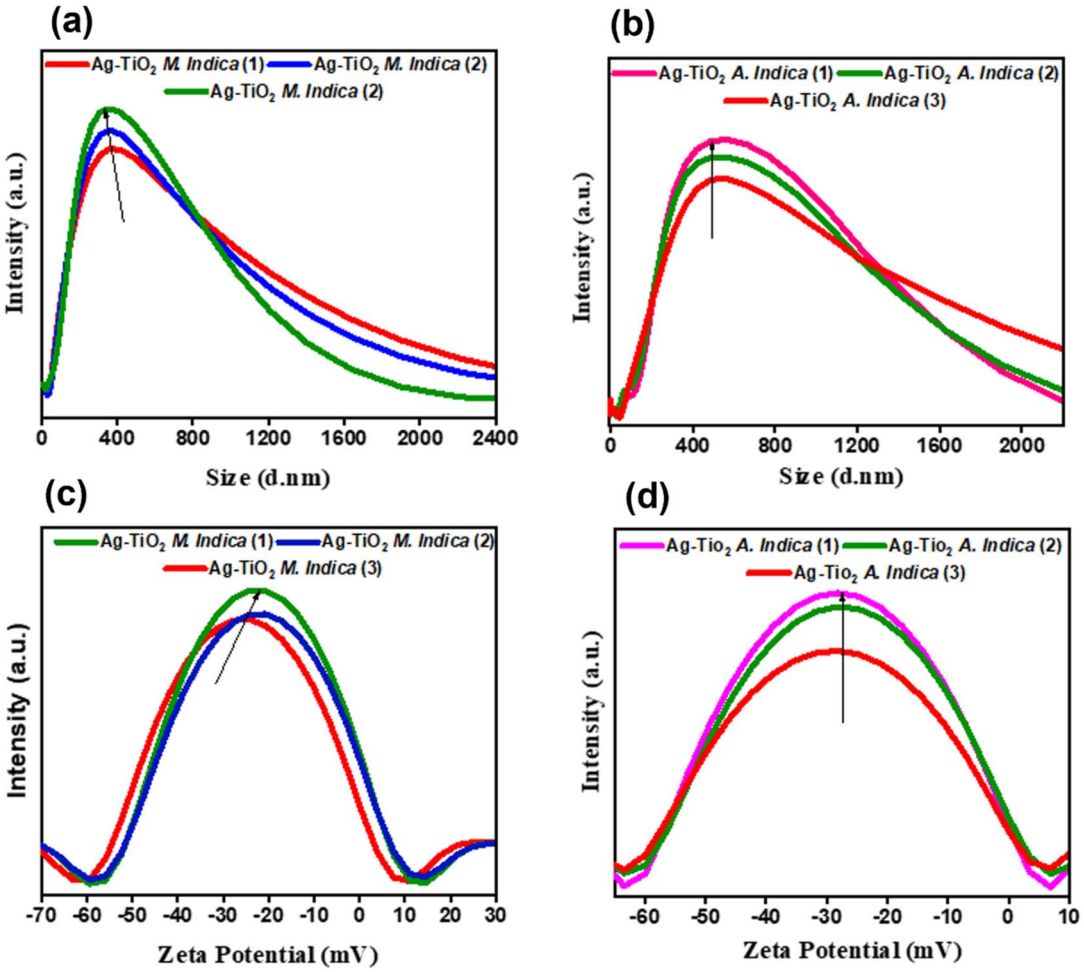

Fig. 4 (a and b) Dynamic light scattering and *Z*-average hydrodynamic diameter of Ag–TiO_2 NCs (*A. indica* and *M. indica*), (c and d) zeta potential measurements for Ag–TiO_2 NCs synthesized using *A. indica* and *M. indica* leaf extracts.

up of small-sized anatase crystallite-size NPs. Similar TiO_2 NPs have already been reported in our previous research paper.[28]

The small particles ranging from 5–8 nm for Ag NPs agree well with the XRD and UV results. The AgNPs were eventually distributed and arranged on the surface of the TiO_2 crystalline particles. The high-resolution TEM (HRTEM) images reveal that the lattice fringes of Ag have a plane spacing of 0.214 nm and 0.209 nm, which matches well with the (200) lattice distance, and the plane spacing of TiO_2 (anatase phase) is about 0.357 and 0.351 nm, which corresponds to the (101) plane, as shown in Fig. 5(c) and (d). These HRTEM parameters agreed with the X-ray diffraction (XRD) spectra. A SAED pattern of Ag–TiO_2 NCs (*A. indica* and *M. indica*) shows the polycrystalline nature of NCs. The observed rings in Fig. 5(e) and (f) are assigned to the (111), (004), (101), (200), and (211) planes of Ag and TiO_2 NPs.

5.7. SEM and EDAX analysis

The particle shape of green synthesized Ag–TiO_2 NCs were studied by SEM analysis which observed the spherical shape of both Ag and TiO_2 NCs. These images show agglomeration (minimum surface free energy) of the particles that exhibit a non-uniform particle distribution Fig. 6(a) and (b). These nanocomposites reported large surface areas, which makes them applicable for nano-medicine applications and also have more catalytic active sites. The elemental composition of Ag–TiO_2 NCs was determined by EDAX analysis and confirmed the presence of Ag (silver), Ti (titanium), and O (oxygen), as shown in Fig. 6(a) and (b).

5.8. Antimicrobial activity and determination of MIC of Ag–TiO_2 NCs

The minimum inhibitory concentration of Ag–TiO_2 NCs (*A. indica* and *M. indica*) against *Escherichia coli* and *Staphylococcus aureus* is tabulated below. Both Ag–TiO_2 NCs (*A. Indica* and *M. Indica*) with a MIC <2500 μg mL^{-1} were considered for testing against two Gram-positive bacteria (*S. aureus* & *S. hominins*), two Gram-negative bacteria (*E. coli* & *S. typhimurium*) and yeast (*C. albicans*). These NCs were active with the concentration (MIC <2500 μg mL^{-1}) against the mentioned microbes shown in Table 1. Based on the spectrum of the pathogens and the MIC, the activity is best in Ag–TiO_2 NCs (*A. indica*) compared to Ag–TiO_2 NCs (*A. indica*).

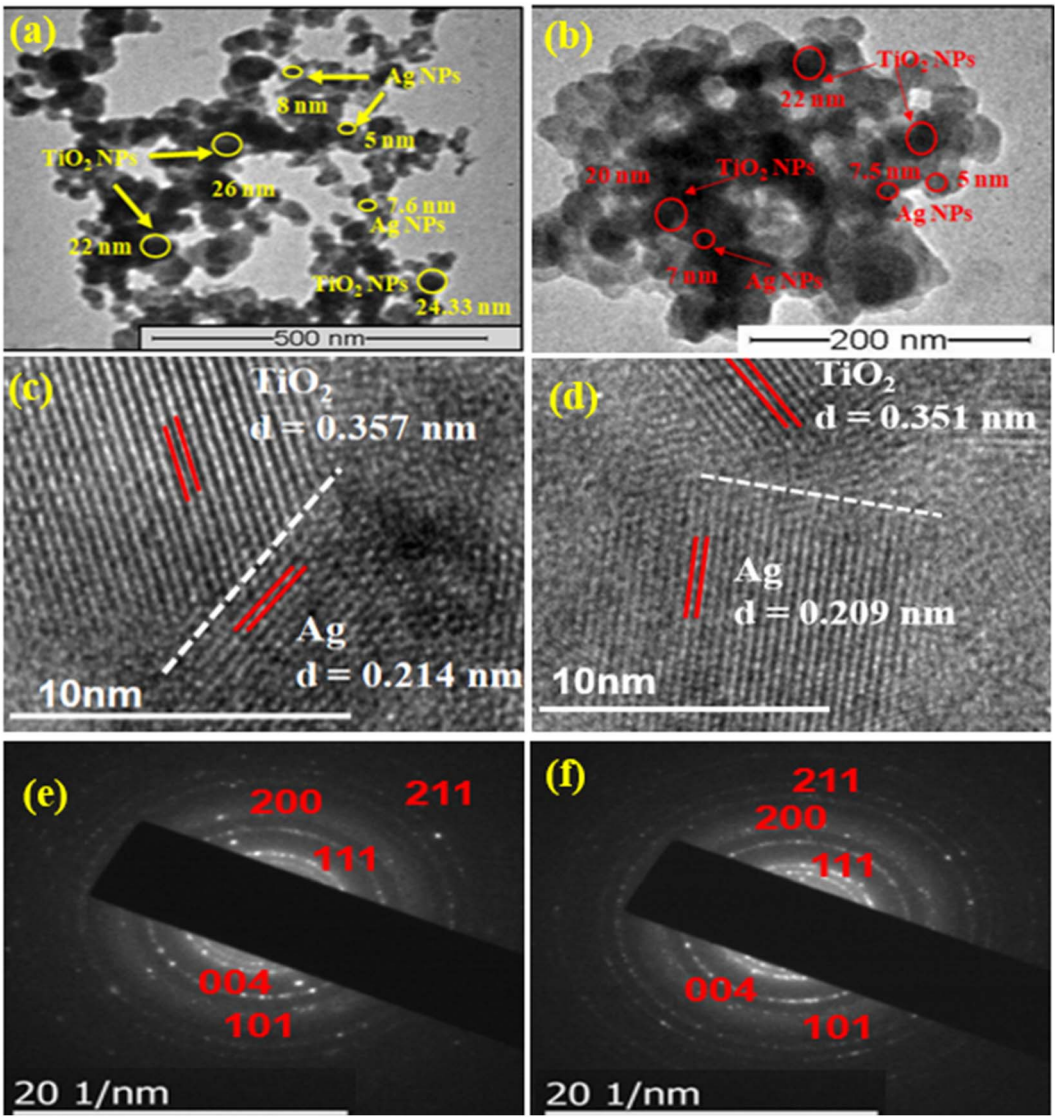

Fig. 5 (a and b) TEM images (c and d) HRTEM images (e and f) SAED images of Ag–TiO_2 NCs synthesized using *A. indica* and *M. indica* leaf extracts.

6. *In vitro* cytotoxicity of ATN and ATM in rat fibroblast cells

We evaluated the effect of ATN and ATM on the cytotoxicity and cell viability at three different concentrations (1/2×, 1×, and 2× of MIC) using the MTT assay in fibroblast cells. The results show that ATN and ATM did not affect the cell viability at any of the given concentrations, for up to 2× of MIC, as represented in Fig. 7(a) and (b). This suggests that ATN and ATM are non-toxic to fibroblast cells at the evaluated concentration of 2× of MIC.

7. Acute and sub-acute dermal toxicity

Based on the above performed antimicrobial tests, we chose 1×, 5× and 10× of MIC, *i.e.*, (625 μg mL^{-1}, 3125 μg mL^{-1} and 6250 μg mL^{-1}) for dermal toxicity. We observed that acute and sub-dermal toxicity testing of Ag–TiO_2 (*A. indica* and *M. indica*) NCs at up to 10× MIC in the CF rats did not cause any significant edema and erythema in the treated skin area in acute and sub-acute dermal toxicity (ESI: Fig. S1b.† Images of acute) (ESI: Fig. S1b.† Images of sub-acute). The erythema and edema in skin responses are each rated on a 0–4 scale individually. The irritation index was used to calculate the sum of the scores for erythema and edema. The primary irritation was calculated for each dose as the difference between the irritation index test site and control site, as reported by Kojic *et al.*[44] There was no sign of irritation and primary irritation index. These results show that Ag–TiO_2 is safe for short-term usage at up to 10× MIC. There was no significant skin damage or irritation, even with the compound used reputedly for 28 days. There was no significant behavioural change observed throughout the experiment.

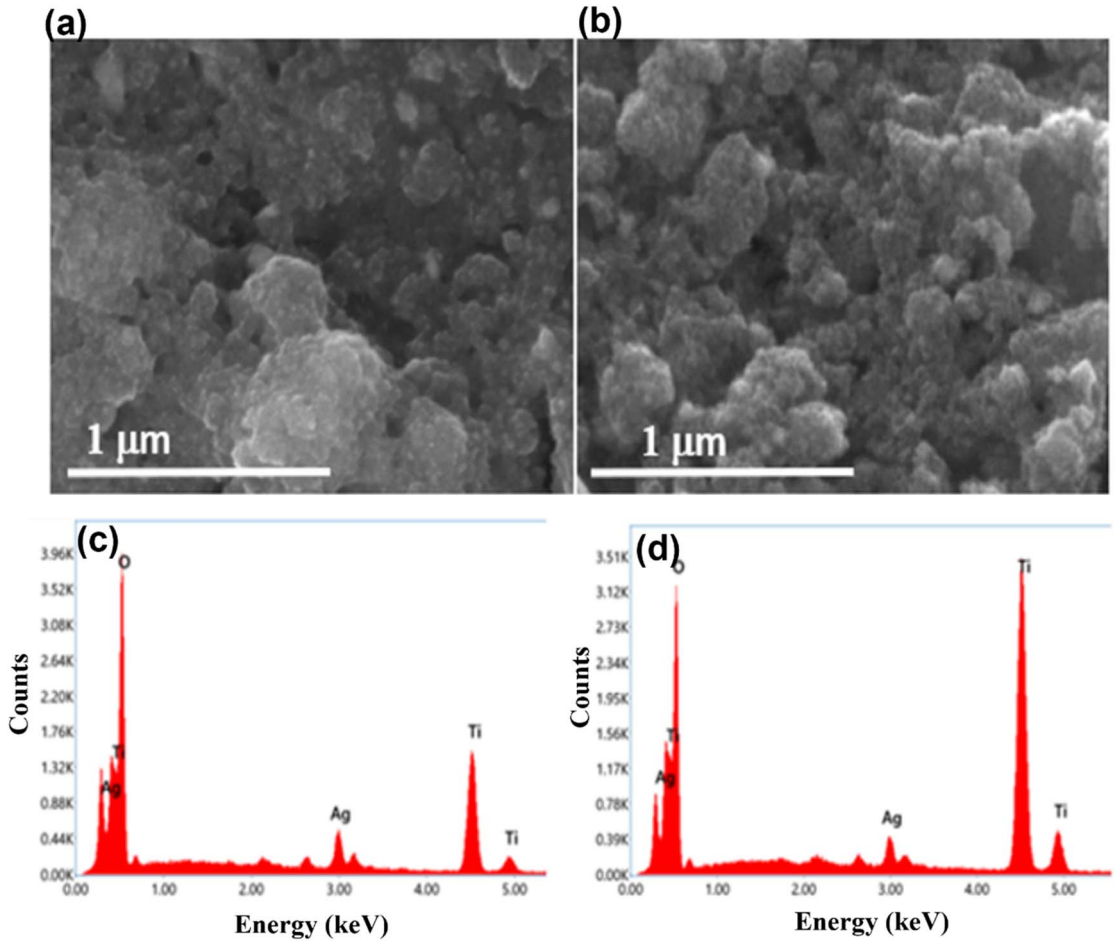

Fig. 6 (a and b) SEM images and (c and d) EDAX spectra of green-synthesized Ag–TiO_2 NCs (*A. indica* and *M. indica*).

Table 1 MICs of Ag–TiO_2 NCs (*A. indica* and *M. indica*)

Sample	*Staphylococcus aureus* (μg mL^{-1})	*Staphylococcus hominis* (μg mL^{-1})	*Escherichia coli* (μg mL^{-1})	*Salmonella typhimurium* (μg mL^{-1})	*Candida albicans* (μg mL^{-1})
MI	2500	2500	2500	2500	1250
AI	2500	2500	2500	2500	1250
ATM	**312.5**	2500	**625**	2500	**1250**
ATN	**625**	2500	**625**	2500	**312**
Vancomycin	0.0625	0.062	—	—	
Ofloxacin	—	—	≤0.0012	≤0.0017	—
Clotrimazole	—	—	—	—	≤0.0019

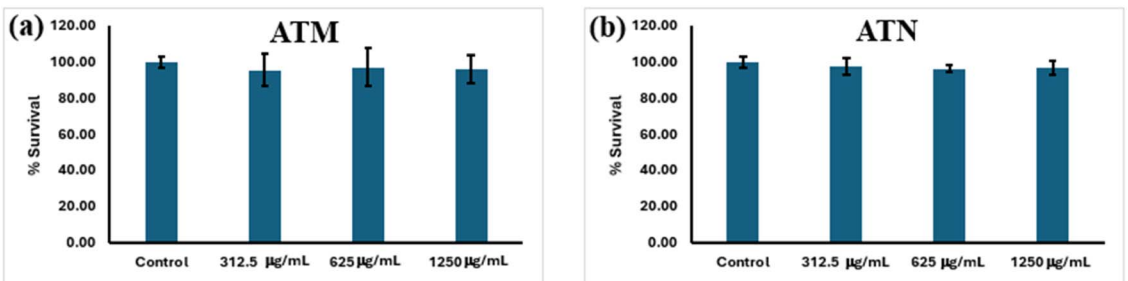

Fig. 7 (a and b) Percent cell viability of rat fibroblast cells treated with ATN and ATM (1/2×, 1×, and 2× of MIC) compared with the vehicle-treated cells using MTT [3-(4,5-dimethylthiazol-2-yl)-diphenyltetrazolium bromide] (mean ± SEM ($n = 4$)).

Table 2 Irritation index (II) of Ag–TiO_2 NCs (*A. indica*) at 1×, 5×, and 10× of MIC (625 μg mL^{-1}, 3125 μg mL^{-1} and 6250 μg mL^{-1}) when applied once dermally for 28 days

Day	Control (sesame oil)	Ag–TiO_2 NCs (1× MIC)	Ag–TiO_2 NCs (5× MIC)	Ag–TiO_2 NCs (10× MIC)
0	0	0	0	0
3	0	0.75	0.5	0.5
7	0	0.75	0.25	0.25
11	0	0.75	0.75	0.5
14	0	0.75	0.5	0.5
17	0	1	0.5	0.75
21	0	0.25	0.75	1
24	0	1	0.75	0.5
28	0	0.75	1.75	1.5

7.1. Behavioural changes

The results from Ag–TiO_2 NCs (*A. indica* and *M. indica*) upon dermal application to CF rats are presented in Tables 2–5. The rats did not exhibit any significant behavioural abnormalities, skin effects, respiratory issues, difficulties in consuming food, or water, hair loss, or posture alignment.

7.2. Haematological, serum biochemical parameters and oxidative stress

The haematological profile was performed to understand whether the compound was causing any abnormalities. There were no significant changes observed in the total body weight, RBC, and WBC counts, as shown in Fig. S2(a) and (b).† Serum biochemistry also showed no substantial changes in the treated animals compared to the control. The cholesterol level, serum albumin, total serum protein, triglycerides, *etc.*, were comparable with the control group shown in S1, Tables 1 and 2.† No significant ($p > 0.05$) changes were observed in the biochemical parameters.

Nanomaterials are a developing technology with applications in science, and nanostructures are important tools within different areas of the field. However, there are various health hazards and environmental issues with chemically and physically synthesized NPs, and they are very expensive. A wide range of research has been carried out, and an alternative method has evolved, *i.e.*, green synthesis of the NCs. Medicinal plants are usually considered safe due to their natural occurrences. However, the toxicity and adverse effects of medicinal plant-based nanomaterials or composites need to be studied for regulatory clearances and their industrial application. Hence, we felt it was compulsory to perform *in vivo* dermal safety evaluation experiments for industrial uses to provide proven scientific evidence. Nowadays, dermal care products are gaining attention as individuals are showing greater interest in them. To present scientific evidence on environmental and health safety problems, this research incorporates both technical and societal difficulties.[45]

Nanomaterials have been studied *via* inhalation and oral and dermal routes based on biomedical needs.[46] Due to the unpredictability and ease of NCs exposure in typical applications, the dermal exposure route was selected amidst the possibilities.[47] AgNPs are being utilized in cosmetic consumer products, have the highest level of commercialization, and are employed in 30% of items that contain nanomaterials.[48]

The skin of rats was sensitized for 28 days, but no erythema or edema were observed (Tables 2 and 3). PII was also between 0–1, which means that the prepared $AgTiO_2$ NCs is safe to use in cosmetics for a short period (Tables 4 and 5). Acute and sub-acute toxicity help us to understand the toxic behaviour of compounds, and help to evaluate the morphological and physiological changes in the body.

For the acute toxicity test, Ag–TiO_2 NCs were left on rat's skin with different concentrations (625 mg mL^{-1} (1×), 3125 mg mL^{-1} (5×), and 6250 mg mL^{-1} (10×)) for 24 h, and there were

Table 3 Primary irritation index (PII) of Ag–TiO_2 NCs (*A. indica*) at 1×, 5×, and 10× of MIC when applied once dermally for 28 days

Day	Ag–TiO_2 NCs (1× MIC)	Ag–TiO_2 NCs (5× MIC)	Ag–TiO_2 NCs (10× MIC)
0	0	0	0
3	0.75	0.5	0.5
7	0.75	0.75	0.25
11	0.75	0.75	0.5
14	0.75	0.5	0.5
17	1	0.75	0.75
21	0.25	0.75	1
24	1	0.75	1.75
28	0.75	0.5	1.5

Table 4 Irritation index (II) of Ag–TiO_2 NCs (*M. indica*) at 1×, 5×, and 10× of MIC when applied once dermally for 28 days

Day	Control (sesame oil)	Ag–TiO_2 NCs (1× MIC)	Ag–TiO_2 NCs (5× MIC)	Ag–TiO_2 NCs (10× MIC)
0	0	0	0	0
3	0	0.75	0.5	0.5
7	0	0.75	0.25	0.25
11	0	0.75	0.75	0.5
14	0	0.75	0.5	0.5
17	0	1	0.5	0.75
21	0	0.25	0.75	1
24	0	1	0.75	0.5
28	0	0.75	1.75	1.5

Table 5 Primary irritation index (PII) of Ag–TiO_2NCs (*M. indica*) at 1×, 5×, and 10× of MIC when applied once dermally for 28 days

Day	Ag–TiO_2 NCs (1× MIC)	Ag–TiO_2 NCs (5× MIC)	Ag–TiO_2 NCs (10× MIC)
0	0	0	0
3	0.75	0.5	0.75
7	0.75	0.75	0.25
11	0.75	0.5	0.75
14	0.75	0.5	0.5
17	1	0.5	0.75
21	0.25	0.75	1
24	0.75	1	1
28	1.25	1.25	1.5

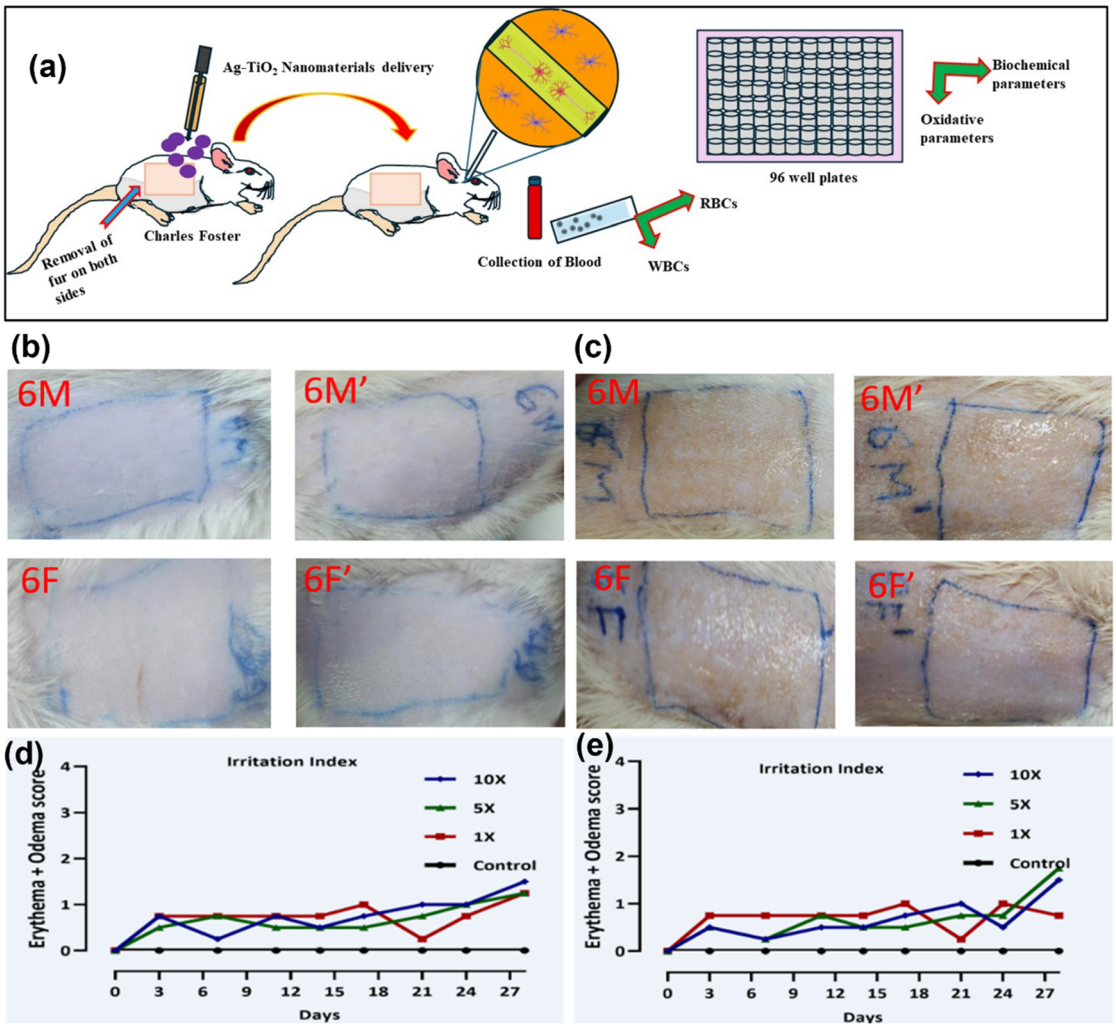

Fig. 8 (a) Illustration of the nanomaterial toxicity in Charles Foster species, (b and c) observation of high doses of Ag–TiO_2 NCs (derived from different plants), and (d and e) irritation index of both *A. indica* and *M. indica* Ag–TiO_2 NC samples.

no significant changes in the body weight and no skin irritation was observed in the rats. Furthermore, the sub-acute toxicity test after 28 days of Ag–TiO_2 NCs exposure on the skin with the above-mentioned concentration did not induce any skin irritation, as observed in Fig. S3(a) and (b).† The body weight, biochemical, and oxidative stress parameters, with repeated administration of Ag–TiO_2 NCs, were applied and compared with the control animals (applied only sesame oil) (S1 Tables 1 and 2†). The depiction of nanomaterials in Charles Foster rats has been studied using biochemicals, oxidative parameters, and irritation index, as illustrated in Fig. 8(a)–(e). The toxic traits of the current $AgTiO_2$ NCs are represented in Fig. 8(a), from removing fur of CF rats to testing for WBCs, RBCs, and other parameters. Fig. 8(b) and (c) shows the first and last day of $AgTiO_2$ NCs formulation on CF rats. Similarly, Fig. 8(d) and (e) depicts the irritation index behaviour of $AgTiO_2$ NCs after 28 days.

Based on the experimental observations, it is evident that the $AgTiO_2$ NCs can be used in cosmetics and topical formulations. However, further clinical studies are required to validate and ensure the safety and efficacy of $AgTiO_2$ NCs. NCs are essential to be used as a scientifically verified product. A thorough physicochemical characterization is crucial for establishing the link between NPs and toxicological reactions.[49] These statistics provide basic information about NPs that may be applied to risk evaluation in nanosafety. Modern techniques, including TEM, XRD, UV-vis, DLS, FTIR, and zeta-potential, were employed to evaluate the morphology, crystallinity, particle size, functional groups, and surface charge for Ag–TiO_2 NCs identification. They may have an impact on Ag–TiO_2 NCs toxicity.[50] Shaaban *et al.* mentioned that the AgNPs hydrogel formulation with a 2% addition showed wound healing of the skin without any side effects of erythema, edema, or irritation and hence can be well corroborated with the current observation.[51]

8. Conclusion

The results of this investigation demonstrate that Ag–TiO_2 NCs synthesized using *A. indica* and *M. indica* leaf extract have shown no harmful effects on animals during dermal

application. We evaluated the effect of ATN and ATM on the cytotoxicity and cell viability at three different concentrations (1/2×, 1×, and 2× of MIC) using the MTT assay in fibroblast cells showing no toxic behaviour up to 2× of MIC. Rats treated with different doses of Ag–TiO_2 NCs (1×, 5×, and 10×) exhibited no side effects or abnormal symptoms over 4 weeks, as confirmed by the irritation index. Moreover, haematological, biochemical, and oxidative stress assessments revealed no differences between the control and treatment groups. Based on these findings, it can be concluded that green-synthesized Ag–TiO_2 NCs in concentrations up to 10× of MIC (6250 μg mL^{-1}) can be deemed safe for use in rat models for cosmetics and drug delivery. However, further investigation is necessary to evaluate the long-term exposure effects of green-synthesized Ag–TiO_2 NCs in cosmetics and medical treatments.

Data availability

Raw data were generated at the National Physical Laboratory, Pusa Road, Delhi and Central Institute of Medicinal and Aromatic Plants, Lucknow, Uttar Pradesh.

Author contributions

Archana Rana: conceptualization, writing – original draft, methodology, investigation; Shweta Parashar: formal analysis, supervision, investigation; Diksha Singh and Kavita Singh: formal analysis, investigation; Debabrata Chanda: resources, validation, research, software; Anirban Pal: resources, validation, research, software; Ritu Srivastava: supervision, and validation; Shailesh Narain Sharma: supervision, validation, conceptualization and editing.

Conflicts of interest

The authors declare no conflict of interest.

Acknowledgements

The author Archana Rana would like to thank the University Grants Commission (UGC-90802) for granting a Research Fellowship, as well as AcSIR for providing the resources needed for conducting this experiment.

References

1 A. C. Santos, J. Marto, R. Cha-Cha and A. M. Martins, Nanotechnology-based sunscreens-a review, *Mater. Today Chem.*, 2022, **23**, 100709.
2 A. Rana, A. K. Chaudhary, *et al.*, An Investigation of antimicrobial activity for plant pathogens by green-synthesized silver nanoparticles using Azadirachata indica and Mangifera indica, *Physchem*, 2023, **3**, 125–146.
3 P. L. Sanches, L. R. O. Geaquinto, R. Cruz, D. C. Schuck, M. Lorencini, J. M. Granjeiro and A. R. L. Ribeiro, Toxicity Evaluation of TiO_2 Nanoparticles on the 3D Skin Model: A Systematic Review, *Front. Bioeng. Biotechnol.*, 2020, **8**, 575.
4 Y. Liang, A. Simaiti, M. Xu, S. Lv, H. Jiang, X. He, Y. Fan, S. Zhu, B. Du, W. Yang, X. Li and P. Yu, Antagonistic Skin Toxicity of Co-Exposure to Physical Sunscreen Ingredients Zinc Oxide and Titanium Dioxide Nanoparticles, *Nanomaterials*, 2022, **12**(16), 2769.
5 G. M. Nair, T. Sajini and B. Mathew, Advanced green approaches for metal and metal oxide nanoparticles synthesis and their environmental applications, *Talanta Open*, 2022, **5**, 1000800.
6 A. Rana, S. Pathak, D. K. Lim, *et al.*, Recent Advancements in Plant- and Microbe-Mediated Synthesis of Metal and Metal Oxide Nanomaterials and Their Emerging Antimicrobial Applications, *ACS Appl. Nano Mater.*, 2023, **6**(10), 8106–8134.
7 D. Kwek, D. Yu, M. I. Setyawati, A. Gautam, S. S. Adav, E. C. Cheong and K. W. Ng, Understanding the toxicological effects of TiO2 nanoparticles extracted from sunscreens on human keratinocytes and skin explants, *Part. Fibre Toxicol.*, 2024, **21**(1), 1–16.
8 M. Nilavukkarasi, S. Vijaykumar, M. Kalaskar, N. Gurav, S. Gurav, P. K. Praseetha and L. Cappariszeylanica, conjugated TiO_2 nanoparticles as bio-enhancers for antimicrobial and chronic wound repair, *Biochem. Biophys. Res. Commun.*, 2022, **623**, 127–132.
9 S. Li, J. Zeng, D. Yin, P. Liao and S. Ding, Synergic fabrication of titanium dioxide incorporation into heparin-polyvinyl alcohol nanocomposite: enhanced *in vitro* antibacterial activity and care of *in vivo* burn injury, *Mater. Res. Express*, 2021, **8**, 085012.
10 Y. Y. Ho, D. S. Sun and H. H. Chang, Silver Nanoparticles Protect Skin from Ultraviolet B-Induced Damage in Mice, *Int. J. Mol. Sci.*, 2020, **21**(19), 7082.
11 G. Chinnasamy, S. Chandrasekharan, T. W. Koh and S. Bhatnagar, Synthesis, Characterization, Antibacterial and Wound Healing Efficacy of Silver Nanoparticles From Azadirachta indica, *Front. Microbiol.*, 2021, **12**, 611560.
12 J. S. Kim, K. S. Song, J. H. Sung, H. R. Ryu, B. G. Choi, H. S. Cho and I. J. Yu, Genotoxicity, acute oral and dermal toxicity, eye and dermal irritation and corrosion and skin sensitization evaluation of silver nanoparticles, *Nanotoxicology*, 2012, **7**(5), 953–960.
13 K. M. Elattar, F. O. Al-Otibi, M. S. El-Hersh, A. A. Attia, N. M. Eldadamony, A. Elsayed, F. Menaa and W. I. A. Saber, Multifaceted chemical and bioactive features of Ag@ TiO_2 and Ag@ SeO_2 core/shell nanoparticles biosynthesized using Beta vulgaris L. extract, *Heliyon*, 2024, **10**(7), e28359.
14 N. Abbasi, H. Ghaneialvar and R. Moradi, Formulation and characterization of a novel cutaneous wound healing ointment by silver nanoparticles containing *Citrus lemon* leaf: A chemobiological study, *Arabian J. Chem.*, 2021, **14**(7), 103246.
15 A. I. Nicoara, V. L. Ene, B. B. Voicu, M. A. Bucur, I. A. Neacsu, B. S. Vasile and F. Iordache, Biocompatible Ag/Fe-Enhanced TiO_2 Nanoparticles as an Effective Compound in Sunscreens, *Nanomaterials*, 2020, **10**(3), 570.
16 M. Saraswati, R. L. Permadani, A. Slamet, *et al.*, The innovation of antimicrobial and self-cleaning using Ag/

TiO_2 nanocomposite coated on cotton fabric for footwear application, *IOP Conf. Ser.:Mater. Sci. Eng.*, 2021, **509**, 012091.

17 Y. Hou, A. Mushtaq, Z. Tang, E. Dempsey, Y. Wu, *et al.*, ROS-responsive Ag-TiO_2 hybrid nanorods for enhanced photodynamic therapy of breast cancer and antimicrobial applications, *J. Sci.:Adv. Mater. Devices*, 2022, **7**(2), 100417.

18 S. M. Gupta and M. Tripathi, A review of TiO_2 nanoparticles, *Chin. Sci. Bull.*, 2011, **56**, 1639–1657.

19 Y. Zhang, F. Fu, Y. Li, D. Zhang and Y. Chen, One-Step Synthesis of Ag@TiO_2 Nanoparticles for Enhanced Photocatalytic Performance, *Nanomaterials*, 2018, **8**(12), 1032.

20 F. Khojasteh, M. R. Mersagh and H. Hashemipour, The influences of Ni, Ag-doped TiO_2 and SnO_2, Ag-doped SnO_2/TiO_2 nanocomposites on recombination reduction in dye synthesized solar cells, *J. Alloys Compd.*, 2022, **890**, 161709.

21 G. J. Nohynek, E. Antignac, T. Re and H. Toutain, Safety assessment of personal care products/cosmetics and their ingredients, *Toxicol. Appl. Pharmacol.*, 2010, **243**, 239–259.

22 D. J. Dheaa and S. A. Mahdi, Photodynamic therapy and TiO_2-decorated Ag nanoparticles: Implications for skin cancer treatment, *Rev. Compos. Mater. Av.*, 2023, **33**(6), 393–398.

23 M. Ahamed, M. A. M. Khan, M. J. Akhtar, *et al.*, Ag-doping regulates the cytotoxicity of TiO_2 nanoparticles *via* oxidative stress in human cancer cells, *Sci. Rep.*, 2017, **7**, 17662.

24 G. Li, X. Tan, W. Zhao, M. A. I. A'srai and M. H. Razali, In-vitro and in-vivo wound healing studies of Ag@TiO2NRs/GG hydrogel film for skin tissue regeneration, *Mater. Res. Express*, 2023, **10**, 045401.

25 D. Bhardwaj and R. Singh, Green biomimetic synthesis of Ag–TiO_2 nanocomposite using *Origanum majorana* leaf extract under sonication and their biological activities, *Bioresources and Bioprocessing*, 2021, **8**, 1.

26 A. Rana, A. Kumari and A. K. Chaudhary, An investigation of Antimicrobial activity for plant pathogens by Green-Synthesized Silver Nanoparticles using Azadirachata indica and Mangifera indica, *Physchem*, 2023, **3**, 125–146.

27 A. Rana, S. Pathak and K. Kumar, Multifaceted Properties of TiO2 Nanoparticles Synthesized via Mangifera indica and Azadirachta indica Plant Extracts: Antimicrobial, Antioxidant, and Non-linear Optical Investigations for Sustainable Agriculture Applications, *Mater. Adv.*, 2024, **5**, 2767.

28 S. Srivastava, R. K. Lal, K. Yadav, Y. Pant, L. Bawitlung, P. Kumar and C. S. Chanotiya, Chemical composition of phenylpropanoid rich chemotypes of Ocimumbasilicum L. and their antimicrobial activities, *Ind. Crops Prod.*, 2022, **183**, 114978.

29 J. C. Stockert, A. Blázquez-Castro, M. Cañete, R. W. Horobin and Á. Villanueva, MTT assay for cell viability: Intracellular localization of the formazan product is in lipid droplets, *Acta Histochem.*, 2012, **114**(8), 785–796.

30 A. D. Ankomah, Y. D. Boakye, T. A. Agana, V. E. Boamah, P. P. S. Ossei, F. Adu and C. Agyare, Evaluation of Dermal Toxicity and Wound Healing Activity of *Cnestis ferruginea* Vahl ex DC, *Adv. Pharmacol. Pharm. Sci.*, 2022, 5268613.

31 A. Rana, A. K. Chaudhary, S. Saini, R. Srivastava, M. Kumar and S. N. Sharma, Ultrafast transient absorption spectroscopic (UFTAS) and antibacterial efficacy studies of phytofabricated silver nanoparticles using Ocimum Sanctum leaf extract, *Inorg. Chem. Commun.*, 2023, **147**, 110233.

32 Y. Zhang, F. Fu, Y. Li, D. Zhang and Y. Chen, One-Step Synthesis of Ag@TiO2 Nanoparticles for Enhanced Photocatalytic Performance, *Nanomaterials*, 2018, **8**(12), 1032.

33 T. N. Rao, Riyazuddin, P. Babji, N. Ahmad, *et al.*, Green synthesis and structural classification of *Acacia nilotica* mediated-silver doped titanium oxide (Ag/TiO_2) spherical nanoparticles: Assessment of its antimicrobial and anticancer activity, *Saudi J. Biol. Sci.*, 2019, **26**, 1385–1391.

34 F. Caputo, J. Clogston, L. Calzolai, M. Rösslein and A. Prina-Mello, Measuring particle size distribution of nanoparticle enabled medicinal products, the joint view of EUNCL and NCI-NCL. A step-by-step approach combining orthogonal measurements with increasing complexity, *J. Controlled Release*, 2019, **299**, 31–43.

35 D. Bhardwaj, R. Singh, *et al.*, Green biomimetic synthesis of Ag–TiO_2 nanocomposite using Origanummajorana leaf extract under sonication and their biological activities, *Bioresources and Bioprocessing*, 2021, **8**, 1.

36 H. Iqbal, A. Razzaq, B. Uzair, N. Ul Ain, S. Sajjad, N. A. Althobaiti, A. E. Albalawi, B. Menaa, M. Haroon, M. Khan, N. U. Khan and F. Menaa, Breast Cancer Inhibition by Biosynthesized Titanium Dioxide Nanoparticles Is Comparable to Free Doxorubicin but Appeared Safer in BALB/c Mice, *Materials*, 2021, **14**(12), 3155.

37 X. H. Yang, H. T. Fu, X. C. Wang, J. L. Yang, X. C. Jiang and A. B. Yu, Synthesis of silver-titanium dioxide nanocomposites for antimicrobial applications, *J. Nanopart. Res.*, 2014, **16**(8), 2526.

38 S. P. Lim, S. Mehmood and P. Rameshkumar, Amperometric detection of hydrogen peroxide and its density functional theory for adsorption on Ag/TiO2 nanohybrid, *J. Mater. Sci.:Mater. Electron.*, 2020, **31**(8), 6017–6026.

39 B. Govindan and A. R. Soliman, Sol-Gel-Assisted Microwave-Derived Synthesis of Anatase Ag/TiO2/GO Nanohybrids toward Efficient Visible Light Phenol Degradation, *Catalysts*, 2017, **7**(5), 133.

40 M. M. Zahornyi, N. I. Tyschenko, T. F. Lobunets, O. F. Kolomys, V. V. Strelchuk and K. S. Naumenko, The Ag influence on the surface states of TiO_2, Optical activity and its cytotoxicity, *J. Nano- Electron. Phys.*, 2021, **13**(6), 06009.

41 T. Ali, A. Ahmed, U. Alam, I. Uddin, P. Tripathi and M. &Muneer, Enhanced photocatalytic and antibacterial activities of Ag-doped TiO_2 nanoparticles under visible light, *Mater. Chem. Phys.*, 2018, **212**, 325–335.

42 T. N. Rao, Riyazuddin, P. Babji, N. Ahmad, *et al.*, Green synthesis and structural classification of *Acacia nilotica* mediated-silver doped titanium oxide (Ag/TiO_2) spherical

nanoparticles: Assessment of its antimicrobial and anticancer activity, *Saudi J. Biol. Sci.*, 2019, **26**, 1385–1391.

43 S. Bhutani, T. Kalaivani and P. Anilkumar, Synthesis of Ag decorated TiO 2 nanoparticles for ammonia gas sensor application, *J. Environ. Nanotechnol.*, 2021, **10**, 25–34.

44 Z. Kojic, D. Stojanovic, S. Popadic, M. Jokanovic and D. Janackovic, The irritative property of a-tricalcium phosphate to the rabbit skin, *Gen. Physiol. Biophys.*, 2009, **28**, 168–173.

45 S. A. S. Nurul, H. Hazilawati, R. S. Mohd, *et al.*, Subacute Oral Toxicity Assesment of Ethanol Extract of Mariposa christiavespertilionis Leaves in Male Sprague Dawley Rats, *Toxicol. Res.*, 2018, **34**, 85–95.

46 Y. Li and E. Cummins, Hazard characterization of silver nanoparticles for human exposure routes, *J. Environ. Sci. Health, Part A: Toxic/Hazard. Subst. Environ. Eng.*, 2020, **55**(6), 704–725.

47 D. B. Warheit and E. M. Donner, Risk assessment strategies for nanoscale and fine-sized titanium dioxide particles: Recognizing hazard and exposure issues, *Food Chem. Toxicol.*, 2015, **1**(85), 138–147.

48 R. Gautam, S. Yang, A. Maharjan, J. Jo, M. Acharya, Y. Heo and C. Kim, Prediction of Skin Sensitization Potential of Silver and Zinc Oxide Nanoparticles Through the Human Cell Line Activation Test, *Frontiers in Toxicology*, 2021, **3**, 649666.

49 K. Rasmussen, H. Rauscher, A. Mech, J. R. Sintes, D. Gilliland, M. González, P. Kearns, K. Moss, M. Visser, M. Groenewold and E. A. Bleeker, Physico-chemical properties of manufactured nanomaterials-Characterisation and relevant methods. An outlook based on the OECD Testing Programme, *Regul. Toxicol. Pharmacol.*, 2018, **92**, 8–28.

50 J. McClements and D. J. McClements, Standardization of nanoparticle characterization: methods for testing properties, stability, and functionality of edible nanoparticles, *Crit. Rev. Food Sci. Nutr.*, 2016, **56**(8), 1334–1362.

51 S. Shaaban, M. S. S. Adam and N. M. EI-Metwaly, Novel organoselenium-based N-mealanilic acid and its zinc (II) chelate: Catalytic, anticancer, antimicrobial, antioxidant, and computational assessments, *J. Mol. Liq.*, 2022, **363**, 119907.